Title
The impact of remineralization depth on the air–sea carbon balance

Journal
Nature Geoscience, 2(9)

ISSN
1752-0894

Authors
Kwon, Eun Young
Primeau, François
Sarmiento, Jorge L

Publication Date
2009-09-01

DOI
10.1038/ngeo612

LETTERS
PUBLISHED ONLINE: 30 AUGUST 2009 | DOI: 10.1038/NGEO612
nature geoscience

The impact of remineralization depth on the air–sea carbon balance

Eun Young Kwon[1]*, François Primeau[2] and Jorge L. Sarmiento[1]

As particulate organic carbon rains down from the surface ocean it is respired back to carbon dioxide and released into the ocean's interior. The depth at which this sinking carbon is converted back to carbon dioxide—known as the remineralization depth—depends on the balance between particle sinking speeds and their rate of decay. A host of climate-sensitive factors can affect this balance, including temperature[1], oxygen concentration[2], stratification, community composition[3,4] and the mineral content of the sinking particles[5]. Here we use a three-dimensional global ocean biogeochemistry model to show that a modest change in remineralization depth can have a substantial impact on atmospheric carbon dioxide concentrations. For example, when the depth at which 63% of sinking carbon is respired increases by 24 m globally, atmospheric carbon dioxide concentrations fall by 10–27 ppm. This reduction in atmospheric carbon dioxide concentration results from the redistribution of remineralized carbon from intermediate waters to bottom waters. As a consequence of the reduced concentration of respired carbon in upper ocean waters, atmospheric carbon dioxide is preferentially stored in newly formed North Atlantic Deep Water. We suggest that atmospheric carbon dioxide concentrations are highly sensitive to the potential changes in remineralization depth that may be caused by climate change.

The downward flux of particulate organic carbon, F, at a depth z below the base of the euphotic zone z_c is often represented by the power law function $F(z) = F(z_c) \times (z/z_c)^{-b}$ (ref. 6) where the exponent b controls the efficiency of transfer of particulate organic carbon to depth. The global mean value of the exponent b estimated using ocean biogeochemical tracer data is 0.9–1.0 (refs 7–9). Sediment trap observations indicate that the downward transfer efficiency may vary regionally and temporally[10] with the exponent b ranging from 0.5 to 2.0 (refs 4, 11–14). Previous studies using three-dimensional global ocean biogeochemistry models showed that the remineralization depth has an important role in controlling the global distributions of nutrients and carbon[7,8]. In ref. 7, a large change in atmospheric pCO_2 (partial pressure of carbon dioxide) of ~100 ppm was obtained when the exponent b was changed from 0.9 to 2.0. We show here that even a small change in remineralization depth results in a substantial change in atmospheric pCO_2 and we explore the underlying mechanisms of this large sensitivity.

We performed a systematic sensitivity analysis of the distributions of nutrients and carbon to changes in remineralization depth using a 3D global ocean biogeochemistry model[8] (see the Methods section) coupled with a one-box model of the atmosphere. Because the response of the new production of organic matter to nutrient supply is uncertain, we bracketed the ocean's response to changes in the remineralization profile by considering two extreme cases: a 'nutrient-restoring' model where new production depends entirely on the supply of nutrients to the surface ocean by advection and mixing and a 'constant-export' model where new production is kept fixed unless the PO_4 concentration in the production zone drops to zero (see the Methods section). The latter model is more appropriate if new production is limited by external factors such as light or micronutrient input from wind-blown dust[15].

The effect of changing remineralization depth on the distribution of nutrients is illustrated in Fig. 1a. With increase in the remineralization depth, respired nutrients are delivered deeper in the water column, leading to a net transfer of PO_4 from the upper ocean to the deeper ocean. The largest PO_4 increase is in the bottom waters of the North Pacific Ocean whereas North Atlantic Deep Water (NADW) shows a pronounced decrease in PO_4. The maximum PO_4 increase in the deep North Pacific Ocean reflects the increased accumulation of respired nutrients in the deep branch of the global overturning circulation[9]. The reduction of PO_4 in newly formed NADW can also be understood in terms of the interaction of the global overturning circulation and the shift of respired nutrients from intermediate to bottom waters. The upper branch of the Great Ocean Conveyor[16] carries intermediate waters with reduced nutrient concentrations into the North Atlantic Ocean[17] where it is then exported southward as NADW (Fig. 1b). NADW therefore has the effect of decreasing the inventory of preformed PO_4 (biologically unused PO_4 transported from the surface) in the deep ocean (Supplementary Fig. S1).

The downward shift of respired nutrients results in an increased global mean concentration of remineralized PO_4, although export production of organic material either decreases or does not change (Fig. 2a,b). The pool of remineralized PO_4 increases because the mean residence time of remineralized nutrients in the ocean's interior increases[18]. Assuming a constant stoichiometric ratio of C:P, the increase in remineralized PO_4 implies an increase in the pool of respired carbon, which, in turn, implies a decrease in atmospheric pCO_2 (refs 19, 20). Our simulations show substantial variations in atmospheric pCO_2 associated with the rearrangement of the PO_4 distribution (Fig. 2c). For example, pCO_2 decreases by 86 ppm in the nutrient-restoring model and by 185 ppm in the constant-export model as the exponent b changes from 1.4 to 0.5.

We can associate the exponent b with the remineralization e-folding depth, the depth by which 63% of organic matter exported from the euphotic layer has become remineralized. Figure 2d shows that the sensitivity of atmospheric pCO_2 is strongest for e-folding depth scales of less than a few hundred metres. Because the present best estimate for the exponent b, which corresponds to an e-folding depth of 210 m, lies well within the high sensitivity range, a small perturbation of the remineralization depth from its present value can lead to a considerable change in the air–sea carbon partitioning. For example a change of the e-folding depth from 204 to 228 m

[1]Atmospheric and Oceanic Sciences Program, Princeton University, New Jersey 08544, USA, [2]Department of Earth System Science, University of California, Irvine, California 92697, USA. *e-mail: ekwon@princeton.edu.

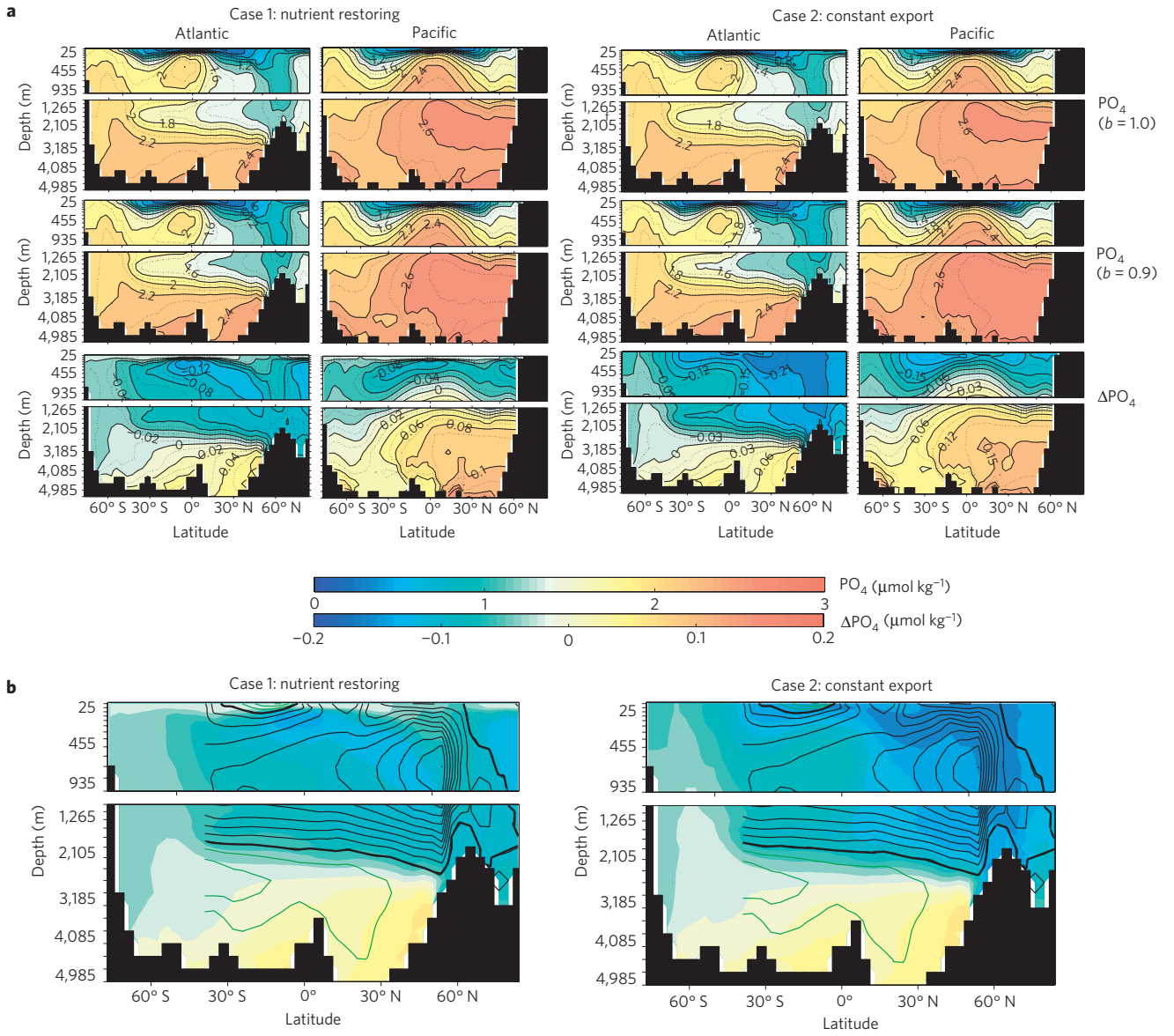

Figure 1 | The response of the PO_4 distribution to an increase in remineralization depth. a, Zonally averaged steady-state PO_4 (μmol kg^{-1}) along the Atlantic and Pacific oceans obtained using the exponents $b = 1.0$ (top) and $b = 0.9$ (middle) and the difference between the two panels (bottom). The e-folding depth changes from 204 to 228 m. **b**, The Atlantic meridional overturning stream function superimposed on the PO_4 difference from **a**. The contour interval of the stream function is 2 Sv (10^6 m^3 s^{-1}). Black lines indicate clockwise circulation. Green lines indicate anticlockwise circulation. The thick black line corresponds to the zero contour line.

in the nutrient-restoring model leads to a decrease in atmospheric pCO_2 of 10 ppm and the same change in the constant-export model leads to a decrease of 27 ppm.

To elucidate the mechanisms by which a deepening of the remineralization depth leads to carbon uptake, we divide the total response of dissolved inorganic carbon (ΔDIC) into contributions from the soft-tissue pump (ΔDIC^{soft}), the carbonate pump (ΔDIC^{carb}) and the gas-exchange pump (ΔDIC^{gasx} (refs 8, 21); see the Methods section). ΔDIC^{soft} and ΔDIC^{carb} represent the changes in DIC that would occur if there were only organic carbon and calcium carbonate ($CaCO_3$) fluxes, respectively, in the absence of air–sea gas exchange. Because the soft-tissue and carbonate pumps (as defined in ref. 21) only rearrange DIC within the ocean, the global integrals of ΔDIC^{soft} and ΔDIC^{carb} are zero. The remaining ΔDIC^{gasx} therefore reveals the distribution of the excess atmospheric CO_2 taken up by the ocean. We also divide the total response of alkalinity into contributions from the soft-tissue and carbonate pumps[8] (see the Methods section) to help understand the causes of carbon uptake.

Figures 3 and 4 illustrate how an increase in the remineralization depth affects the air–sea carbon balance through changes in the soft-tissue and carbonate pumps. An increase in the remineralization depth results in redistributing ΔDIC^{soft} from relatively well-ventilated waters to ones that are poorly ventilated. At the same time, surface alkalinity increases due to a reduction in remineralized nitrate in the upper ocean. The decrease in surface DIC and the increase in surface alkalinity both cause the ocean to take up CO_2 from the atmosphere.

A weakening of the carbonate pump also contributes to carbon uptake when the remineralization depth increases. With increased remineralization depth, the amount of $CaCO_3$ exported from the production zone decreases globally at the same rate as the reduction of particulate organic carbon export (Fig. 2b and Methods). The reduced production of $CaCO_3$ results in increased carbonate ion

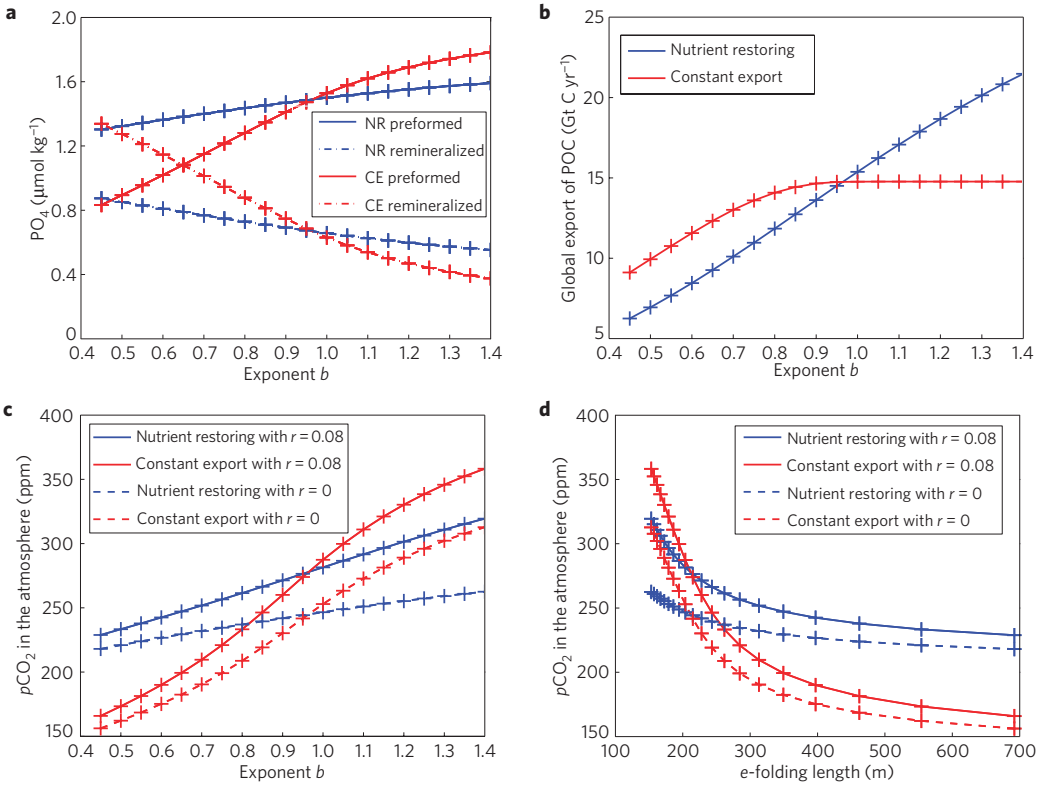

Figure 2 | Sensitivities to changes in remineralization depth. a, The sensitivity of the volume-averaged concentrations of preformed and remineralized PO_4 (μmol kg^{-1}) for the nutrient-restoring model (NR) and the constant-export model (CE). **b**, The sensitivity of the export production as particulate organic carbon (POC) at the base of euphotic layer (Gt C yr^{-1}). **c**, The sensitivity of atmospheric pCO_2 (ppm) obtained using the rain ratio of $CaCO_3$ to POC, $r = 0.08$ (solid lines) and $r = 0$ (dashed lines). **d**, Same as **c** except that the *x*-axis is scaled with respect to the e-folding depth. '+' marks each model data point.

concentrations in the upper ocean and decreased concentrations in the deeper ocean. This rearrangement causes the ocean to take up CO_2 due to the increase in surface alkalinity.

The mechanism mediated by the soft-tissue pump accounts for ~85% of the pCO_2 drawdown in the constant-export model and ~50% in the nutrient-restoring model (Fig. 2c,d). With the $CaCO_3$ cycle turned off, for example, an increase in the remineralization e-folding depth from 204 to 228 m leads to decreases of atmospheric pCO_2 by 23 ppm for the constant-export model and 5 ppm for the nutrient-restoring model. The CO_2 uptake mediated by the soft-tissue pump is about five times greater in the constant-export model, where new production decreases minimally in response to a reduction in surface nutrients.

The global ocean increases its capacity for CO_2 when the remineralization depth increases. Figure 3 shows that increases in ΔDIC^{gasx} are particularly pronounced in the water formed in the high-latitude North Atlantic Ocean. The increased accumulation of respired nutrients in old bottom waters is balanced by the depletion of preformed nutrients in newly formed NADW, which causes carbon accumulation taken in NADW. A net transfer of carbonate ions from old bottom waters to NADW also contributes to CO_2 uptake in the NADW formation regions. As a result, NADW provides a major pathway of atmospheric CO_2 to the deep ocean when the remineralization depth increases globally (Fig. 3b; see also Supplementary Information).

The Southern Ocean has been recognized as a region within which the efficiency of the biological pump controls atmospheric pCO_2. Owing to inefficient biological consumption of surface nutrients, water masses ventilated from the Southern Ocean are characterized by high concentrations of preformed nutrients (average 1.6 μmol kg^{-1} of PO_4 compared to 0.9 μmol kg^{-1} in NADW)[19]. Thus an increased biological use of surface nutrients leads to net uptake of carbon primarily through bottom waters formed in the Southern Ocean[22]. However, increasing remineralization depth does not deplete surface nutrients in the Southern Ocean as much as it does in the NADW formation regions. This is because Circumpolar Deep Water with increased respired carbon upwells and mixes with the surface water, resulting in only a moderate change in surface chemistry. Consequently, bottom waters ventilated from the Southern Ocean are less efficient than NADW at storing atmospheric CO_2 when the remineralization depth increases.

It is noteworthy that the regions within which changes in the remineralization depth control atmospheric pCO_2 are globally distributed. We performed experiments in which we restricted the change in the remineralization depth to individual basins. We found that 38% of the total reduction in atmospheric pCO_2 can be attributed to the increase in the remineralization depth in the Pacific Ocean and that 22%, 21% and 19% can be attributed to those in the Southern Ocean (south of 40° S) and the Atlantic and Indian oceans respectively. The basin-to-basin differences in the sensitivity of atmospheric pCO_2 to a change in the remineralization depth are due to differences in the amount of particulate organic carbon export in each basin (see Supplementary Information).

Palaeoclimate records suggest that respired carbon and nutrients were shifted from intermediate waters towards deep waters in the glacial ocean[23–25]. The shift could have been due to changes in circulation[25] and/or changes in biological production and remineralization[23]. If we ignore the possible differences in the circulation and attribute the shift to a deepening of remineralization, perhaps caused by a slowdown of bacterial consumption of sinking organic matter at colder temperatures[1] or increased ballast minerals[5] in a dustier climate[26], the implied change in remineralization depth corresponds to an increase in the e-folding depth from 204 to 313 m (see Supplementary Information). Figure 2

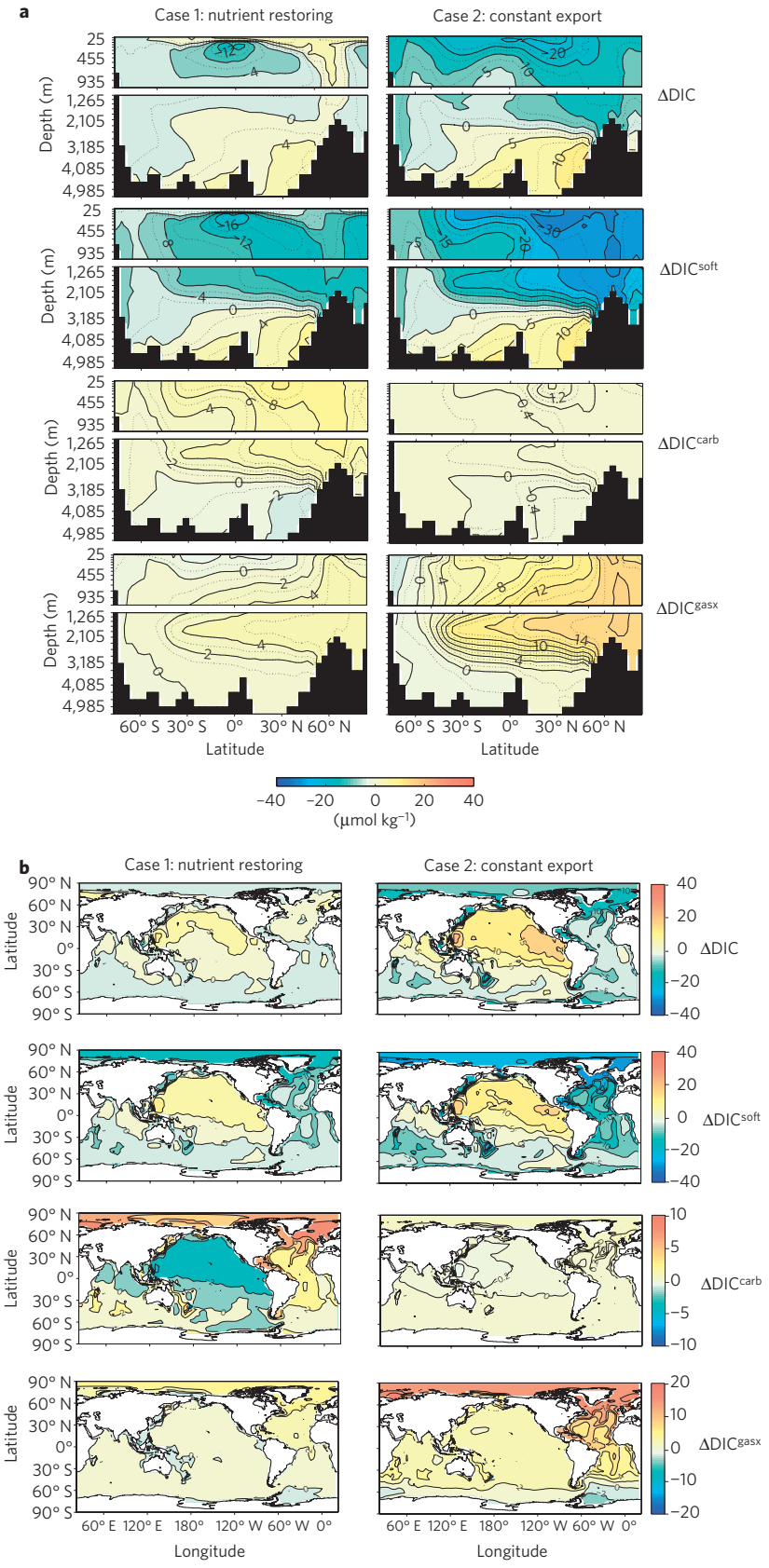

Figure 3 | The DIC response decomposed into soft-tissue, carbonate and gas-exchange pump components. The response of DIC (μmol kg^{-1}) to an increase in the e-folding depth from 204 to 228 m (the exponent *b* changes from 1.0 to 0.9). The total change in DIC (first row) is separated into contributions from the soft-tissue (second row), carbonate (third row) and gas-exchange (fourth row) pumps. **a**, Zonally averaged fields along the Atlantic Ocean. **b**, Depth-averaged fields in the global ocean. Warm colours (positive values) represent an increase in DIC (μmol kg^{-1}). Cold colours (negative values) represent a decrease.

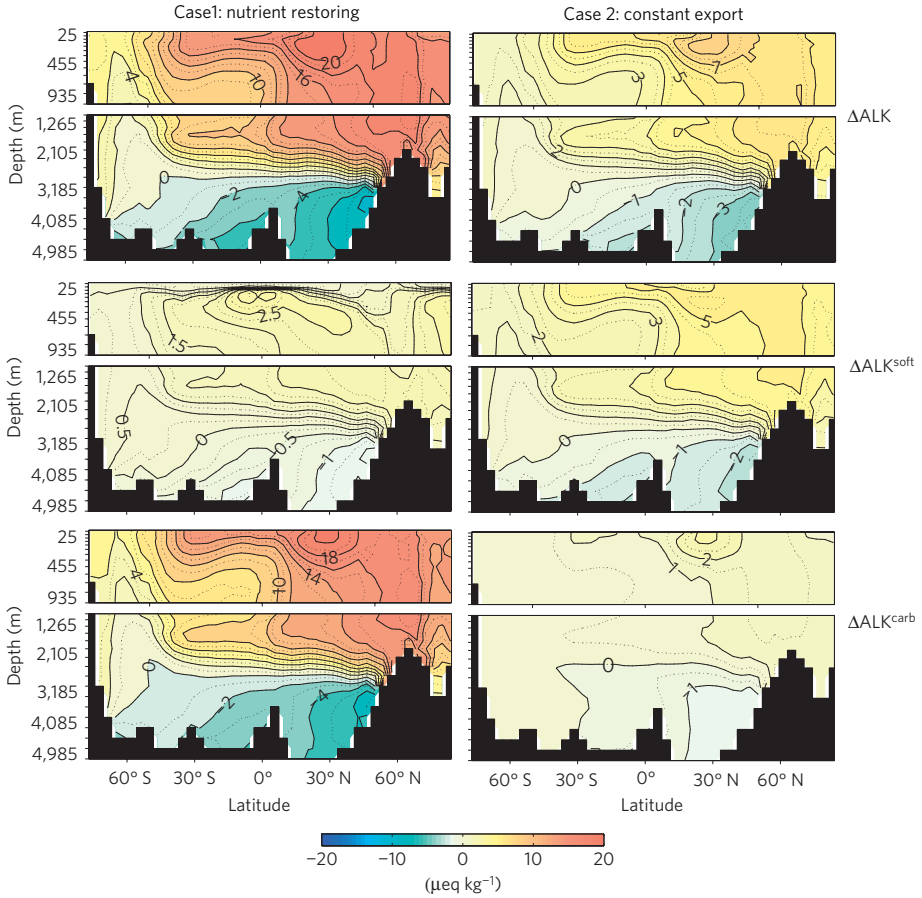

Figure 4 | The alkalinity response decomposed into soft-tissue and carbonate pump components. The response of alkalinity (μeq kg^{-1}) to an increase in the e-folding depth from 204 to 228 m (the exponent b changes from 1.0 to 0.9). The total change in alkalinity (first row) is separated into contributions from the soft-tissue (second row) and carbonate (third row) pumps. Zonally averaged fields along the Atlantic are shown for the nutrient-restoring model and the constant-export model. Warm colours (positive values) represent an increase in alkalinity. Cold colours (negative values) represent a decrease.

suggests that this increase in the remineralization depth leads to a decrease of 30–77 ppm in atmospheric pCO_2 due to the rearrangement of nutrients and alkalinity within the ocean. In an open system where bottom water remineralization interacts with $CaCO_3$ sediments, the downward shift of respired carbon would result in dissolving more $CaCO_3$ sediment and hence in increasing the inventory of alkalinity. This would lead to a further decrease in atmospheric pCO_2 (refs 27, 28).

Climate-change-induced changes in remineralization depth might also influence the oceanic uptake of anthropogenic carbon in the future. A transient simulation shows that considerable fractions (more than 30%) of the full response occur on timescales of decades, although it takes several thousands of years to reach equilibrium (Supplementary Fig. S3). This indicates that possible changes in remineralization depth could feed back on twenty-first century climate change. How remineralization depth will respond to future climate change is uncertain at present, but our work suggests that the impact on the global carbon cycle could be substantial.

Methods

Global ocean biogeochemistry model. The OCMIP-2 (ocean carbon-cycle model intercomparison project phase 2; ref. 29) ocean biogeochemistry model is coupled with an off-line primitive equation ocean general circulation model[8,9,18]. This model uses Newton's method to solve for steady-state solutions and hence is several orders of magnitude faster than a traditional approach based on time stepping. The time efficiency allows us to perform a systematic analysis of the model for changes in remineralization depth for which the ocean takes several thousand years to reach equilibrium (Supplementary Fig. S3).

In this model, net community production is simulated by restoring model PO_4 towards observations in the top 75 m of the ocean only when model PO_4 exceeds observations. 74% of the net production becomes dissolved organic matter (DOM) whereas the remaining fraction becomes particulate organic matter (POM). DOM is decomposed to inorganic form with a mean lifetime of 1.7 years. The downward flux of POM follows the power law curve as described by ref. 6. Thus the remineralization of POM, $J(z)$, below the production zone ($z_c = -75$ m) is represented by

$$J(z) = \frac{\partial}{\partial z}\left(\frac{z}{z_c}\right)^{-b} F(z_c)$$

in which $F(z_c)$ is the amount of POM exported from the production zone. The control value of the exponent b is 0.97, the value estimated in ref. 8 using the global PO_4, alkalinity and DIC data. The exponent b can be associated with the e-folding depth, the depth at which the downward flux of POM drops to a factor of 1/e. The corresponding e-folding depths for the exponents b are 153 m ($b = 1.4$), 162 m ($b = 1.3$), 173 m ($b = 1.2$), 186 m ($b = 1.1$), 204 m ($b = 1.0$), 210 m ($b = 0.97$), 228 m ($b = 0.9$), 262 m ($b = 0.8$), 313 m ($b = 0.7$), 397 m ($b = 0.6$) and 554 m ($b = 0.5$).

The $CaCO_3$ production is proportional to the production of particulate organic carbon with a rain ratio of $r = 0.08$. Subsequently $CaCO_3$ dissolves following an exponential curve with an e-folding length scale of 2,100 m, which is fixed throughout this study. This model assumes constant stoichiometric ratios of C:N:P = 137:16:1. All of these 'control' parameter values were determined in ref. 8. There are no sedimentation processes in this model.

Nutrient-restoring model and constant-export model. In the nutrient-restoring model, we follow the nutrient-restoring scheme as implemented in OCMIP-2 (ref. 29) where model-predicted surface nutrients are restored towards observations with a timescale of 30 days only when model PO_4 exceeds the observations. In the constant-export model new production is kept fixed to the value diagnosed from the control run unless the PO_4 concentration in the production zone drops to zero. Where PO_4 is below zero, new production stops.

Preformed and remineralized PO_4. We divide the total PO_4 in the ocean into preformed and remineralized components:

$$PO_4 = PO_4^{pre} + PO_4^{rem}$$

By definition, all PO_4 in the surface ocean is preformed and the preformed PO_4 in the subsurface ocean is the PO_4 that is transported from the surface by ocean circulation. The remineralized PO_4 is the PO_4 that is added to the subsurface water by remineralization of organic material. Here we compute the subsurface preformed PO_4 by integrating the convolution over the entire surface area Ω,

$$PO_4^{pre} = \int_{\Omega} PO_4(r_s) G(r_s)\, d^2 r_s$$

where $PO_4(r_s)$ is the surface concentration of PO_4 and $G(r_s)$ is the volume integrated Green's function denoting the volume of the ocean per unit surface area that is ventilated from the surface grid point, r_s (ref. 18). The remineralized PO_4, PO_4^{rem}, is obtained by subtracting the preformed PO_4 from the total PO_4.

Carbon pump separation and alkalinity pump separation. We apply the carbon pump separation method[21] to the DIC response pattern[8]. Thus the total response of DIC (ΔDIC) becomes

$$\Delta DIC = \Delta DIC^{soft} + \Delta DIC^{carb} + \Delta DIC^{gasx}$$

in which the change in DIC is attributed to the contributions from the soft-tissue pump, the carbonate pump and the gas-exchange pump. The soft-tissue pump component of the DIC response is obtained by multiplying the stoichiometric ratio of C:P by the PO_4 response:

$$\Delta DIC^{soft} = r_{C:P} \times \Delta PO_4 \quad (1)$$

and the carbonate pump component of the DIC response is the nitrate-corrected alkalinity response[30]:

$$\Delta DIC^{carb} = (\Delta ALK + r_{N:P} \times \Delta PO_4)/2 \quad (2)$$

The gas-exchange pump component of the DIC response is obtained by subtracting equations (1) and (2) from the total DIC response.

Likewise the alkalinity response is separated into the contributions from the soft-tissue pump and the carbonate pump[8]. Thus the total response of the alkalinity (ΔALK) becomes

$$\Delta ALK = \Delta ALK^{soft} + \Delta ALK^{carb}$$

where the soft-tissue pump component is estimated as

$$\Delta ALK^{soft} = -r_{N:P} \times \Delta PO_4$$

and the remaining ΔALK becomes the carbonate pump component of the alkalinity response.

Received 27 January 2009; accepted 28 July 2009; published online 30 August 2009

References

1. Matsumoto, K. Biology-mediated temperature control on atmospheric pCO_2 and ocean biogeochemistry. *Geophys. Res. Lett.* **34,** L20605 (2007).
2. Devol, A. H. & Hartnett, H. E. Role of the oxygen-deficient zone in transfer of organic carbon to the deep ocean. *Limnol. Oceanogr.* **46,** 1648–1690 (2001).
3. Klaas, C. & Archer, D. E. Association of sinking organic matter with various types of mineral ballast in the deep sea: Implications for the rain ratio. *Glob. Biogeochem. Cycles* **16,** 1116 (2002).
4. Francois, R., Honjo, S., Krishfield, R. & Manganini, S. Factors controlling the flux of organic carbon to the bathypelagic zone of the ocean. *Glob. Biogeochem. Cycles* **16,** 1087 (2002).
5. Armstrong, R. A., Lee, C., Hedges, J. I., Honjo, S. & Wakeham, S. G. A new, mechanistic model for organic carbon fluxes in the ocean based on the quantitative association of POC with ballast minerals. *Deep-Sea Res. II* **49,** 219–236 (2001).
6. Martin, J. H., Knauer, G. A., Karl, D. M. & Broenkow, W. W. VERTEX: Carbon cycling in the northeast Pacific. *Deep-Sea Res.* **34,** 267–285 (1987).
7. Yamanaka, Y. & Tajika, E. The role of the vertical fluxes of particulate organic matter and calcite in the ocean carbon cycle: Studies using an ocean biogeochemical general circulation model. *Glob. Biogeochem. Cycles* **10,** 361–382 (1996).
8. Kwon, E. Y. & Primeau, F. Optimization and sensitivity of a global biogeochemistry ocean model using combined *in situ* DIC, alkalinity, and phosphate data. *J. Geophys. Res.* **113,** C08011 (2008).
9. Kwon, E. Y. & Primeau, F. Optimization and sensitivity study of a biogeochemistry ocean model using an implicit solver and *in situ* phosphate data. *Glob. Biogeochem. Cycles* **20,** GB4009 (2006).
10. Buesseler, K. O. & Boyd, P. W. Shedding light on processes that control particle export and flux attenuation in the twilight zone of the open ocean. *Limnol. Oceanogr.* **54,** 1210–1232 (2009).
11. Berelson, W. POC fluxes into the ocean interior: A comparison of 4 US-JGOFS regional studies. *Oceanography* **14,** 59–67 (2001).
12. Buesseler, K. O. *et al.* Revisiting carbon flux through the ocean's twilight zone. *Science* **316,** 567–570 (2007).
13. Lutz, M., Dunbar, R. & Caldeira, K. Regional variability in the vertical flux of particulate organic carbon in the ocean interior. *Glob. Biogeochem. Cycles* **16,** 1037 (2002).
14. Conte, M., Ralph, N. & Ross, E. H. Seasonal and interannual variability in deep ocean particle fluxes at the oceanic flux program (OFP)/Bermuda Atlantic Time Series (BATS) site in the western Sargasso Sea near Bermuda. *Deep-Sea Res. II* **48,** 1471–1505 (2001).
15. Sarmiento, J. L., Hughes, T. M. C., Stouffer, R. J. & Manabe, S. Simulated response of the ocean carbon cycle to anthropogenic climate warming. *Nature* **393,** 245–249 (1998).
16. Broecker, W. S. The great ocean conveyor. *Oceanography* **4,** 89–89 (1991).
17. Williams, R. G., Roussenov, V. & Follows, M. J. Nutrient streams and their induction into the mixed layer. *Glob. Biogeochem. Cycles* **20,** GB1016 (2006).
18. Primeau, F. Characterizing transport between the surface mixed layer and the ocean interior with a forward and adjoint global ocean transport model. *J. Phys. Oceanogr.* **35,** 545–564 (2005).
19. Ito, T. & Follows, M. J. Preformed phosphate, soft tissue pump and atmospheric CO_2. *J. Mar. Res.* **63,** 813–839 (2005).
20. Marinov, I., Follows, M. J., Gnandesikan, A., Sarmiento, J. L. & Slater, R. D. How does ocean biology affect atmospheric pCO_2? Theory and models. *J. Geophys. Res.* **113,** C07032 (2008).
21. Gruber, N. & Sarmiento, J. L. in *The Sea* (eds Robinson, A. R., McCarthy, J. J. & Rothschild, B. J.) 337–399 (Wiley, 2002).
22. Marinov, I., Gnanadesikan, A., Toggweiler, I & Sarmiento, J. L. The southern ocean biogeochemical divide. *Nature* **441,** 964–967 (2006).
23. Boyle, E. A. Vertical oceanic nutrient fractionation and glacial/interglacial CO_2 cycles. *Nature* **331,** 55–56 (1988).
24. Jaccard, S. L. *et al.* Subarctic Pacific evidence for a glacial deepening of the oceanic respired carbon pool. *Earth Planet. Sci. Lett.* **277,** 156–165 (2008).
25. Marchitto, T. M. & Broecker, W. S. Deep water mass geometry in the glacial Atlantic Ocean: A review of constraints from the paleonutrient proxy Cd/Ca. *Geochem. Geophys. Geosyst.* **7,** Q12003 (2006).
26. Mahowald, N. *et al.* Dust sources and deposition during the Last Glacial Maximum and current climate: A comparison of model results with paleodata from ice cores and marine sediments. *J. Geophys. Res.* **104,** 15895–15916 (1999).
27. Sigman, D. M., McCorkle, D. C. & Martin, W. R. The calcite lysocline as a constraint on glacial/interglacial low-latitude production changes. *Glob. Biogeochem. Cycles* **12,** 409–427 (1998).
28. Archer, D., Winguth, A., Lea, D. & Mahowald, N. What caused the glacial/interglacial atmospheric pCO_2 cycles? *Rev. Geophys.* **38,** 159–189 (2000).
29. Najjar, R. G. *et al.* Impact of circulation on export production, dissolved organic matter, and dissolved oxygen in the ocean: Results from phase II of the ocean carbon-cycle model intercomparison project (OCMIP-2). *Glob. Biogeochem. Cycles* **21,** GB3007 (2007).
30. Brewer, P. G., Wong, G. T. F., Bacon, M. P. & Spencer, D. W. An oceanic calcium problem? *Earth Planet. Sci. Lett.* **26,** 81–87 (1975).

Acknowledgements

We thank E. Galbraith and R. Toggweiler for their valuable comments. F.P. acknowledges support from National Science Foundation grant OCE 0623647. E.Y.K. and J.L.S. acknowledge award NA07OAR4310096 from the National Oceanic and Atmospheric Administration, US Department of Commerce. The statements, findings, conclusions and recommendations are those of the authors and do not necessarily reflect the views of the National Oceanic and Atmospheric Administration, or the US Department of Commerce.

Author contributions

E.Y.K. and F.P. initiated the project. E.Y.K. carried out model simulations and analyses with advice from F.P. and J.L.S. E.Y.K. wrote the paper and the Supplementary Information with input from F.P. and J.L.S.

Additional information

Supplementary information accompanies this paper on www.nature.com/naturegeoscience. Reprints and permissions information is available online at http://npg.nature.com/reprintsandpermissions. Correspondence and requests for materials should be addressed to E.Y.K.